2015

Electron-hole diffusion lengths >175 μm in solution-grown $CH_3NH_3PbI_3$ single crystals

Qingfeng Dong
University of Nebraska-Lincoln, qingfeng.dong@gmail.com

Yanjun Fang
University of Nebraska-Lincoln, jkfang@zju.edu.cn

Yuchuan Shao
University of Nebraska-Lincoln

Padhraic Mulligan
Ohio State University

Jie Qiu
Ohio State University

See next page for additional authors

Dong, Qingfeng; Fang, Yanjun; Shao, Yuchuan; Mulligan, Padhraic; Qiu, Jie; Cao, Lei; and Huang, Jinsong, "Electron-hole diffusion lengths >175 μm in solution-grown $CH_3NH_3PbI_3$ single crystals" (2015). *Mechanical & Materials Engineering Faculty Publications*. 194.
https://digitalcommons.unl.edu/mechengfacpub/194

Authors
Qingfeng Dong, Yanjun Fang, Yuchuan Shao, Padhraic Mulligan, Jie Qiu, Lei Cao, and Jinsong Huang

Sciencexpress Reports

Electron-hole diffusion lengths >175 μm in solution-grown $CH_3NH_3PbI_3$ single crystals

Qingfeng Dong,[1]* Yanjun Fang,[1]* Yuchuan Shao,[1]* Padhraic Mulligan,[2] Jie Qiu,[2] Lei Cao,[2] Jinsong Huang[1]†

[1]Department of Mechanical and Materials Engineering, University of Nebraska, Lincoln, NE 68588, USA. [2]Nuclear Engineering Program, Department of Mechanical and Aerospace Engineering, Ohio State University, Columbus, OH 43210, USA.

*These authors contributed equally to this work.

†Corresponding author. E-mail: jhuang2@unl.edu

Long, balanced electron and hole diffusion lengths greater than 100 nanometers in polycrystalline $CH_3NH_3PbI_3$ are critical for highly efficient perovskite solar cells. We report that the diffusion lengths in $CH_3NH_3PbI_3$ single crystals grown by a solution-growth method can exceed 175 μm under 1 sun illumination and exceed 3 mm under weak light for both electrons and holes. The internal quantum efficiencies approach 100% in 3 mm-thick single crystal perovskite solar cells under weak light. These long diffusion lengths result from greater carrier mobility, lifetime and dramatically smaller trap densities in the single crystals than polycrystalline thin-films. The long carrier diffusion lengths enabled the use of $CH_3NH_3PbI_3$ in radiation sensing and energy-harvesting through gammavoltaic effect with an efficiency of 3.9% measured with an intense cesium-137 source.

Demonstrated optoelectronic applications of organolead trihalide perovskites (OTPs) include high-efficiency photovoltaic (PV) cells (*1–3*), lasers (*4*), light-emitting-diodes (*5*), and high gain photodetectors (*6*), but the understanding of their fundamental properties, such as carrier diffusion length, has lagged behind. The carrier diffusion length in $MAPbI_3$ should be sensitive to defects. Point defects in $MAPbI_3$ do not constitute midgap trap states (*7*), but a large density of charge traps has been broadly observed at the grain boundaries and surfaces of $CH_3NH_3PbI_3$ ($MAPbI_3$) polycrystalline (MPC) films (*8*, *9*). We showed that the carrier diffusion length of MPC films increased to 1 μm when solvent annealing was used to enlarge the grain size to the thickness of the film (*10*). To determine the limit of carrier diffusion length, larger $MAPbI_3$ single crystals (MSCs) are needed. We report the growth of millimeter-size MSCs using a low-temperature solution approach and their fundamental electronic property characterization. Both electrons and holes have diffusion lengths >175 μm under 1 sun illumination and >3 mm in MSCs under weak illumination (0.003% sun).

Large-sized MSC growth from a supersaturated $MAPbI_3$ solution used a top-seeded-solution-growth (TSSG) method (fig. S1) with a temperature gradient. Small-sized MSCs at the bottom of the container maintained the MA^+, Pb^{2+}, and I^- ion concentration for a saturated solution, the cooler top half of the solution was supersaturated. The large MSCs were grown by the consumption of small MSCs in the bottom. The small temperature difference from bottom and the top of the solution induces a small convection that is enough to transport the material to the large MSCs. The as-grown MSCs have an average size of 3.3 mm and a largest size of ~10 mm (Fig. 1A); powder x-ray diffraction (XRD) (Fig. 1B) confirmed the tetragonal structure. Single-crystal XRD was best fit with an I4/m space group in agreement with the results of Baikie et al. (*11*). The goodness-of-fit was 1.154, and the crystal data are summarized in tables S1 and S2.

We fabricated MSC PV devices by depositing 25-nm gold (Au) layers on one crystal facet as anodes and contacting gallium (Ga) with the opposite facet as cathodes (Fig. 2A). Thin MSCs with a thickness of 100 to 200 μm were peeled off from the large MSCs to fabricate MSC devices with thicknesses of either >3 mm or 200 μm. The optical and electric properties of MSCs were compared with those of the 600-nm-thick solvent-annealed MPC thin films formed by the interdiffusion method (*10*). The MSC has an extended absorption band to 850 nm while regular MPC thin films have an absorption cutoff at 800 nm (Fig. 2B), which is consistent with the external quantum efficiency (EQE) of devices made of these two types of materials (Fig. 2C). These MSC devices differ from other MPC thin-film devices in that they exhibit a strong exciton absorption at 790 nm that was more intense in the thicker devices. The red-shift of the EQE cutoff by 50 nm to 850 nm in the MSCs increases the upper limit of J_{SC} in $MAPbI_3$-based solar cells from 27.5 mA cm^{-2} to 33.0 mA cm^{-2}. The PL peak of the MSCs (770 nm) has a shorter wavelength than the exciton peak (Fig. 2C), which indicates all of the excitons generated in MSCs dissociate to free charges at room temperature; and the band gap of the MSCs should be 1.61 eV. The blue-shifted and narrower PL peak indicates a lower trap density in MSCs.

The EQE of a 3 mm-thick MSC solar cell (Fig. 2D) ranged from 12.6 to 15.8% for wavelengths from 520 to 810 nm. The EQE of the MSC device decreased for shorter wavelengths,

which suggests the Au/MSC interface contains a large defect density (shorter wavelengths generate carriers closer to the MSC surface). These defects are most likely from the Pb^{2+} clusters formed by partial loss of the more soluble methylammonium iodide (MAI) when the single crystal is removed from solution. Our recent density functional theory calculation verified the Pb^{2+} clusters on the $MAPbI_3$ surface tend to form charge traps (*6*). The internal quantum efficiency (IQE) of the 3-mm MSC device (derived by dividing EQE by the transmittance of the Au electrode; see Fig. 2D and fig. S2) was near unity (95 ± 7%).

The electrons generated in the very thin perovskite layer near the Au anode must traverse the whole crystal to be collected by the Ga cathode, indicating that the electron diffusion length in MSCs is greater than the crystal thickness (~3 mm). We also replaced Ga by a semitransparent Au (25 nm)/C_{60} (25 nm) layer as the cathode so that photogenerated charges would be located at the cathode side. Again, the short circuit current density (J_{SC}) measured at 0.1% Sun was comparable with incident light from both sides, which indicates the hole diffusion length in MSCs is also longer than the MSC thickness.

The dependence of responsivity (R) and J_{SC} on light intensity (I_L) for thick devices are summarized in Fig. 2, E and F, respectively [see fig. S3 for photocurrent density-voltage (J_{ph}-V) curves]. Under 1 Sun, the open circuit voltage V_{oc} was 0.62 V, vs. ~1.00 V in optimized MPC thin film devices again indicating a strong charge recombination in the MSC devices under strong illumination. For thick MSC devices, R decreased from 35 to 0.19 mA W^{-1} when the intensity of white illuminated light increased from for 0.003 to 100 mW cm^{-2} because of increased charge recombination for higher I_L. Fitting of J_{sc} with I_L as $J_{sc} \propto I_L^{\beta}$ gave a β = 0.5 ± 0.01, suggesting that second-order charge recombination dominated in the thick MSC devices for I_L > 0.003 mW cm^{-2} as seen previously (*12*, *13*). Reducing the MSC thickness to 200 μm recovered large R (Fig. 2E) at 1 sun and increased β to 0.88, which indicates the carrier diffusion length of MSCs is near 200 μm for 1 sun illumination.

We could characterize the carrier mobility (μ) and carrier lifetime (τ_r) because the carrier diffusion length (L_D) is determined by $L_D = (k_B T \mu \tau_r / e)^{1/2}$, where k_B, T, and e are the Boltzmann constant, temperature, and elementary charge, respectively. The device dark current (J_D) was measured to derive the trap density and carrier mobilities. The MSCs were sandwiched by two Au electrodes deposited by thermal evaporation to form hole-only devices. As shown in Fig. 3A, the linear J_D-V relation (green line) indicates an Ohmic response at the low bias (< 2.1 V). A trap-filling process was identified by the dramatic increase of the current injection at a bias range of 2.1 to 10.7 V. The voltage at which all the traps are filled (trap-filled limit voltage V_{TFL}) was determined by the trap density (*14*):

$$V_{TFL} = \frac{e n_t L^2}{2\varepsilon\varepsilon_0} \quad (1)$$

where L is the thickness of the MSCs, ε (= 32) is relative dielectric constant of $MAPbI_3$, and ε_0 is the vacuum permittivity. The trap density n_t in MSCs was calculated to be 3.6 × 10^{10} cm^{-3}. For comparison, the hole-only devices with MPC thin films were also fabricated with PEDOT:PSS and Au as the hole injection electrodes (fig. S4). The calculated hole trap density in the MPC thin films was 2.0 × 10^{15} cm^{-3}, which is almost five orders of magnitude greater than in the MSCs. Thermal admittance spectroscopy (TAS) (fig. S5) confirmed the dramatically reduced trap density by 2 to 3 orders of magnitude in MSCs. Thus, the extraordinary carrier diffusion length in the MSCs is the result of largely suppressed trap density. When operating in the trap-free space charge limit current (SCLC) regime above 10.7 V, the dark current of the MSC was well fitted by (blue line) the Mott-Gurney Law:

$$J_D = \frac{9\varepsilon\varepsilon_0 \mu V_b^2}{8L^3} \quad (2)$$

where V_b is applied voltage. A large hole mobility of 164 ± 25 cm^2 V^{-1} s^{-1} was derived from the curve fitting. The uncertainties we reported represent a single standard deviation in the measurements on ten nominally identical devices. Hall effect measurements revealed that the MSC was slightly *p*-doped with a low free hole concentration of (9 ± 2) × 10^9 cm^{-3} (see supplementary materials). The hole mobility from Hall effect measurement was 105 ± 35 cm^2 V^{-1} s^{-1}, agreeing with the SCLC results. Similarly, the electron trap density and electron mobility of MSCs were measured with the electron-only devices which have Phenyl-C_{61}-butyric acid methyl (PCBM):C_{60}/Ga as both electrodes. A low electron trap density of 4.5 × 10^{10} cm^{-3} was derived (Fig. 3B), comparable to the hole trap density, and the electron mobility was 24.8 ± 4.1 cm^2 V^{-1} s^{-1}. Finally, we used time-of-flight (ToF) to verify the high electron mobilities of 24.0 ± 6.8 cm^2 V^{-1} s^{-1} (Fig. 3C). The electron and hole mobilities in MSCs are several fold greater than the intrinsic band transport mobility in MPC thin films (*10*) and polycrystals (*15*) measured by Hall effect method and those measured by transient terahertz spectroscopy (*16*), both of which measure band transport mobility. However, ToF and SCLC mobilities are sensitive to the presence charge traps in the materials. The excellent agreement of Hall mobility with ToF and SCLC mobilities in the single crystal $MAPbI_3$ devices indicates the band-tail states in the OTP single crystals are negligible.

We measured τ_r in MSCs with transient photovoltaic (TPV) and impedance spectroscopy (IS) at different I_L (Fig. 4); at 1 sun, the TPV and IS values of τ_r were 82 ± 5 and 95 ± 8 μs, respectively, more than 10 times longer than that in the best thin film devices with sophisticated surface passivation (*10*). Combining the measured mobility and lifetime

of MSCs, the hole diffusion length is 175 ± 25 μm under 1 sun. The measured bulk carrier lifetime can be underestimated because of the presence of surface charge recombination, so the bulk carrier diffusion length should exceed this value. Reducing the bias light intensity to 0.1 sun increased τ_r to 234 and 198 μs by TPV and IS measurements, respectively.

The long carrier diffusion length of $MAPbI_3$ can find direct application in x-ray and gamma-ray sensing and radiation energy harvesting. Radiation is generally much weaker than 1 sun but should penetrate the entire device. Details pertaining to the carrier diffusion length extrapolation under weak light, radiation measurement, simulation, and the estimation of gammavoltaic efficiency can be found in the supplementary materials. We extrapolated a carrier recombination lifetime of 2.6 ± 0.2 s and carrier diffusion length sum of 33 ± 5 mm under the light intensity 0.003 mW cm^{-2} from our 1 sun data. The presence of surface recombination should reduce the carrier diffusion length, and the measured >3 mm electron and hole diffusion length under weak light is thus reasonable. We exposed the 3 mm thick MSC device to intense gamma-ray and measured the electric current generation. A cesium-137 gamma irradiator of 102 Ci yielded a persistent current of 36.3 ± 0.3 nA, which corresponds to a photon-to-electron conversion efficiency of 3.9% and agrees with the theoretic estimation.

In summary, the demonstrated high carrier mobility, carrier lifetime and diffusion length of the MSCs open several new directions for the application of $MAPbI_3$ materials in printable electronics, lasers and solar cells, respectively (*4*). The high PL quantum yield of $MAPbI_3$ and excellent overlap of the PL spectra with the absorption spectrum of the single crystal allows photon recycling in thick perovskite crystals by reabsorbing the emission (*4*, *5*). The demonstration of a charge diffusion length that greatly exceeds the above band gap photon absorption depth implies that IQE's of essentially 100% can be achieved under the low internal electric fields at max power point.

REFERENCES AND NOTES

1. S. D. Stranks, G. E. Eperon, G. Grancini, C. Menelaou, M. J. Alcocer, T. Leijtens, L. M. Herz, A. Petrozza, H. J. Snaith, Electron-hole diffusion lengths exceeding 1 micrometer in an organometal trihalide perovskite absorber. *Science* **342**, 341–344 (2013). Medline doi:10.1126/science.1243982

2. M. M. Lee, J. Teuscher, T. Miyasaka, T. N. Murakami, H. J. Snaith, Efficient hybrid solar cells based on meso-superstructured organometal halide perovskites. *Science* **338**, 643–647 (2012). Medline doi:10.1126/science.1228604

3. A. Mei, X. Li, L. Liu, Z. Ku, T. Liu, Y. Rong, M. Xu, M. Hu, J. Chen, Y. Yang, M. Grätzel, H. Han, A hole-conductor-free, fully printable mesoscopic perovskite solar cell with high stability. *Science* **345**, 295–298 (2014). Medline doi:10.1126/science.1254763

4. G. Xing, N. Mathews, S. S. Lim, N. Yantara, X. Liu, D. Sabba, M. Grätzel, S. Mhaisalkar, T. C. Sum, Low-temperature solution-processed wavelength-tunable perovskites for lasing. *Nat. Mater.* **13**, 476–480 (2014). Medline doi:10.1038/nmat3911

5. Z. K. Tan, R. S. Moghaddam, M. L. Lai, P. Docampo, R. Higler, F. Deschler, M. Price, A. Sadhanala, L. M. Pazos, D. Credgington, F. Hanusch, T. Bein, H. J. Snaith, R. H. Friend, Bright light-emitting diodes based on organometal halide perovskite. *Nat. Nanotechnol.* **9**, 687–692 (2014). Medline

6. R. Dong *et al*., *Adv. Mater.* 10.1002/adma.201405116 (2015). 10.1002/adma.201405116

7. J. Kim, S. H. Lee, J. H. Lee, K. H. Hong, The role of intrinsic defects in methylammonium lead iodide perovskite. *J. Phys. Chem. Lett.* **5**, 1312–1317 (2014). doi:10.1021/jz500370k

8. N. K. Noel, A. Abate, S. D. Stranks, E. S. Parrott, V. M. Burlakov, A. Goriely, H. J. Snaith, Enhanced photoluminescence and solar cell performance via Lewis base passivation of organic-inorganic lead halide perovskites. *ACS Nano* **8**, 9815–9821 (2014). Medline doi:10.1021/nn5036476

9. I. A. Shkrob, T. W. Marin, Charge trapping in photovoltaically active perovskites and related halogenoplumbate compounds. *J. Phys. Chem. Lett.* **5**, 1066–1071 (2014). doi:10.1021/jz5004022

10. Z. Xiao, Q. Dong, C. Bi, Y. Shao, Y. Yuan, J. Huang, Solvent annealing of perovskite-induced crystal growth for photovoltaic-device efficiency enhancement. *Adv. Mater.* **26**, 6503–6509 (2014). Medline doi:10.1002/adma.201401685

11. T. Baikie, Y. Fang, J. M. Kadro, M. Schreyer, F. Wei, S. G. Mhaisalkar, M. Graetzel, T. J. White, Synthesis and crystal chemistry of the hybrid perovskite $(CH_3NH_3)PbI_3$ for solid-state sensitised solar cell applications. *J. Mater. Chem. A* **1**, 5628–5641 (2013). doi:10.1039/c3ta10518k

12. J. S. Manser, P. V. Kamat, Band filling with free charge carriers in organometal halide perovskites. *Nat. Photonics* **8**, 737–743 (2014). doi:10.1038/nphoton.2014.171

13. S. D. Stranks, V. M. Burlakov, T. Leijtens, J. M. Ball, A. Goriely, H. J. Snaith, Recombination kinetics in organic-inorganic perovskites: Excitons, free charge, and subgap states. *Phys. Rev. A* **2**, 034007 (2014). doi:10.1103/PhysRevApplied.2.034007

14. R. H. Bube, Trap density determination by space-charge-limited currents. *J. Appl. Phys.* **33**, 1733–1737 (1962). doi:10.1063/1.1728818

15. C. C. Stoumpos, C. D. Malliakas, M. G. Kanatzidis, Semiconducting tin and lead iodide perovskites with organic cations: Phase transitions, high mobilities, and near-infrared photoluminescent properties. *Inorg. Chem.* **52**, 9019–9038 (2013). Medline doi:10.1021/ic401215x

16. C. Wehrenfennig, G. E. Eperon, M. B. Johnston, H. J. Snaith, L. M. Herz, High charge carrier mobilities and lifetimes in organolead trihalide perovskites. *Adv. Mater.* **26**, 1584–1589 (2014). Medline doi:10.1002/adma.201305172

17. A. Poglitsch, D. Weber, Dynamic disorder in methylammoniumtrihalogenoplumbates (II) observed by millimeter-wave spectroscopy. *J. Chem. Phys.* **87**, 6373–6378 (1987). doi:10.1063/1.453467

18. B. J. Leever, C. A. Bailey, T. J. Marks, M. C. Hersam, M. F. Durstock, In situ characterization of lifetime and morphology in operating bulk heterojunction organic photovoltaic devices by impedance spectroscopy. *Adv. Energy Mater.* **2**, 120–128 (2012). doi:10.1002/aenm.201100357

19. I. Mora-Seró, G. Garcia-Belmonte, P. P. Boix, M. A. Vázquez, J. Bisquert, Impedance spectroscopy characterisation of highly efficient silicon solar cells under different light illumination intensities. *Energy Environ. Sci.* **2**, 678–686 (2009). doi:10.1039/B812468J

20. M. A. Green, *Solar Cells: Operating Priciples, Technology and System Applications* (Prentice-Hall, Englewood Cliffs, NJ, 1982).

21. R. Devanathan, L. R. Corrales, F. Gao, W. J. Weber, Signal variance in gamma-ray detectors—A review. *Nucl. Instrum. Methods A* **565**, 637–649 (2006). doi:10.1016/j.nima.2006.05.085

ACKNOWLEDGMENTS

We thank the financial support provided by the Department of Energy (Award DE-EE0006709), Defense Threat Reduction Agency (Award HDTRA1-14-1-0030), and the Office of Naval Research (ONR, Award N000141210556). J.H. conceived the idea and supervised the project. Q.D. grew the single crystals and fabricated the devices. Q.D., Y.F., and Y.S. conducted the electric and optical characterization of the devices. P.M., J.Q., and L.C. measured the devices under gamma ray irradiation and did the simulation. J.H. wrote the paper.

SUPPLEMENTARY MATERIALS

www.sciencemag.org/cgi/content/full/science.aaa5760/DC1
Materials and Methods
Figs. S1 to S11
Tables S1 and S2
References (*17*–*21*)

27 December 2014; accepted 20 January 2015
Published online 29 January 2015
10.1126/science.aaa5760

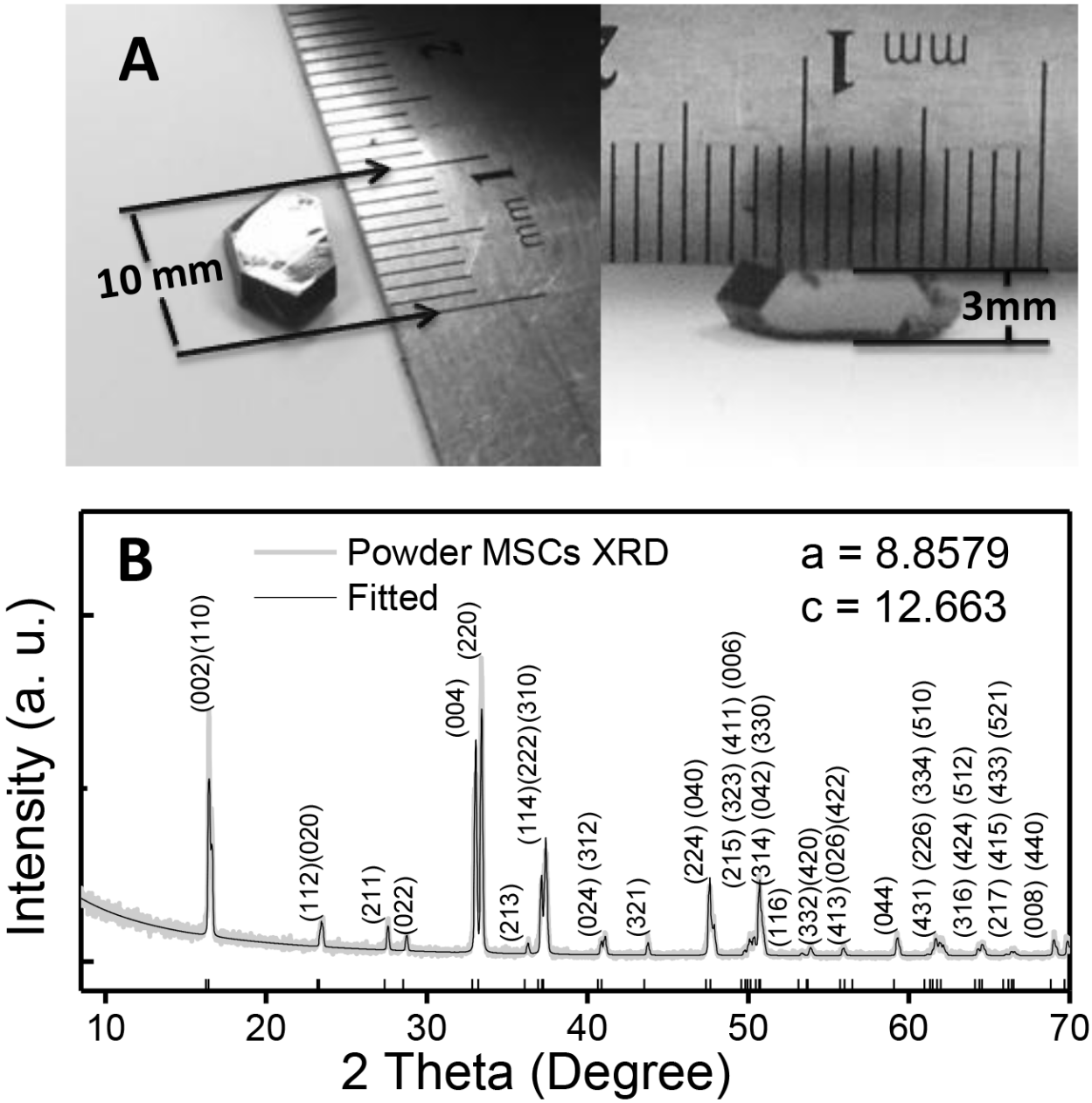

Fig. 1. MSC structure characterization. (**A**) Images of a piece of as-prepared $MAPbI_3$ single crystal. (**B**) X-ray diffraction pattern of the ground powder of a single crystal (gray line) and fitted patterns (black line).

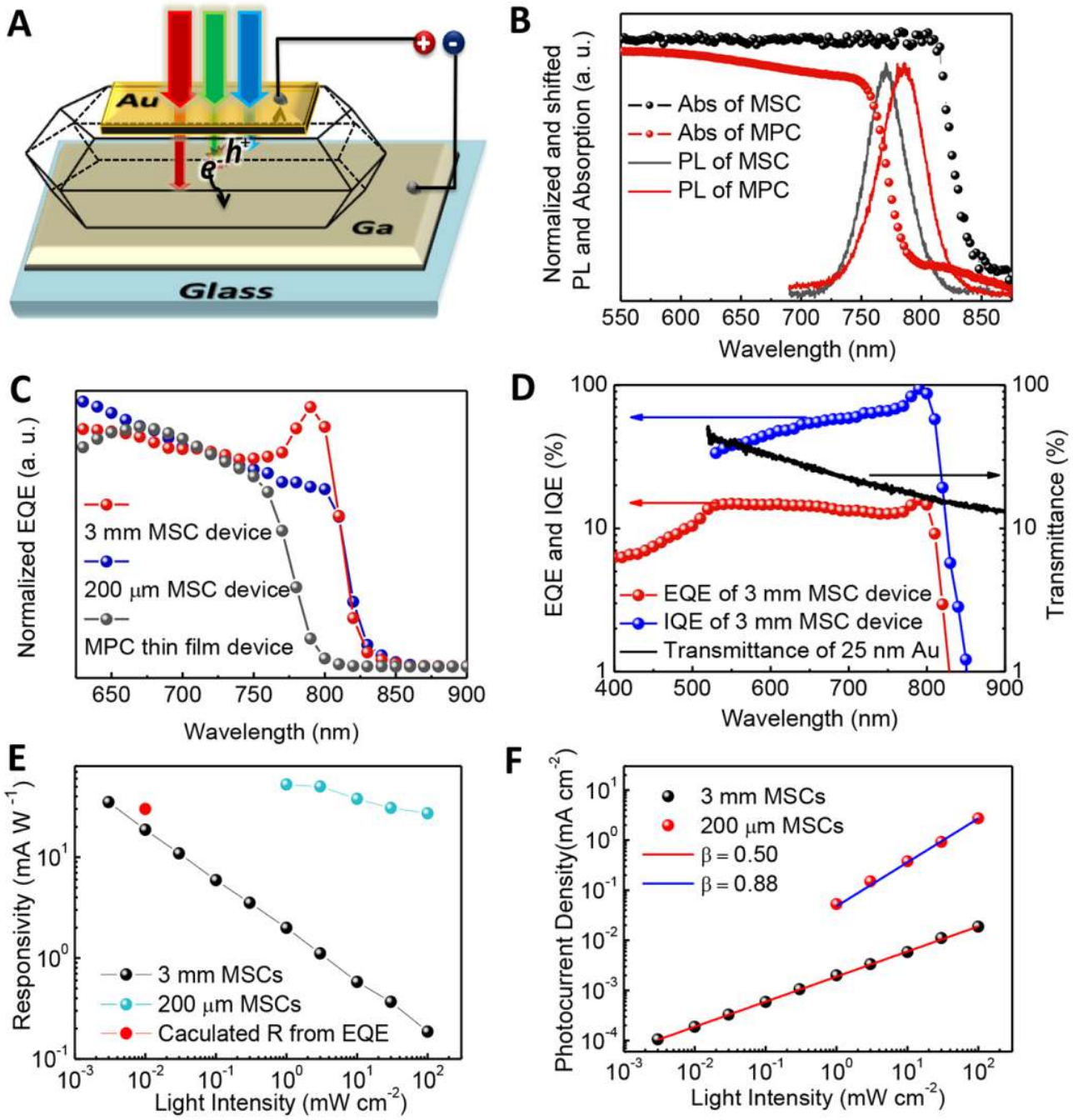

Fig. 2. Device structure and electrical and optical characterization of the MSC devices and MPC thin films. (**A**) Schematic device structure of the $MAPbI_3$ single crystal devices. (**B**) Normalized PL and absorption spectra of the MSCs and MPC thin films. (**C**) Normalized EQE of a 3 mm-thick (red solid line circle) and a 200 μm-thick (blue solid line circle) MSC photovoltaic device, and a MPC thin film device (black solid line circle). (**D**) EQE of a 3 mm-thick MSC device (red solid circle line), the average transmittance of 25 nm Au electrode (black line), and the calculated average IQE (blue solid circle line). (**E**) Responsivity of the 3 mm-thick (black solid circle line) and the 200 μm-thick (blue solid circle line) MSC devices and the responsivity calculated from the EQE of the 3 mm-thick MSC device. (**F**) Current density (J_{sc}) vs light intensity (I_L) fitted by $J_{SC} \propto I_L^{\beta}$ for the MSC devices with a thickness of 3 mm (black solid circle) and 200 μm (red solid circle).

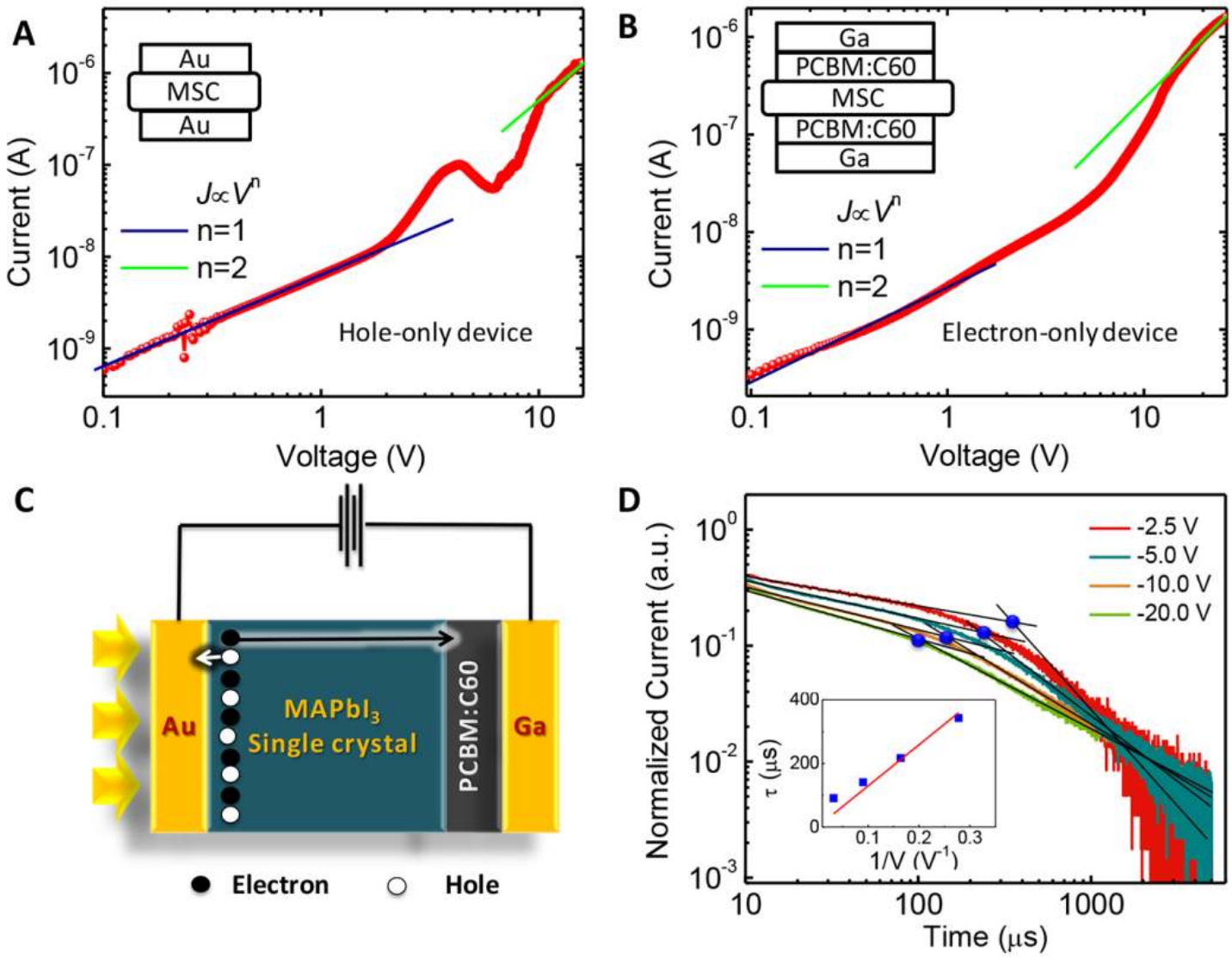

Fig. 3. Carrier mobility characterization of MSCs. Current-voltage curve for a hole-only MSC device (**A**) and an electron-only MSC device (**B**). The insets of (A) and (B) show the device structure of hole-only and electron-only MSC devices, respectively. Three regions can be identified according to different power of n: $n = 1$ is the Ohmic region (fitted by the blue lines), $n = 2$ is the space charge limited current region (fitted by the green lines), and in between is the trap-filled limited region. (**C**) The schematic illustration of the device for the time-of-flight measurement. (**D**) The transient current curves of the MSC device show the normalized transient photocurrent under various reverse biases. The carrier transit time is determined by the intercept of the pretransit and post-transit asymptotes of the photocurrent and marked by solid blue circles. Inset of (D) shows the charge transit time versus the reciprocal of bias, and the solid line is a linear fitting to the data.

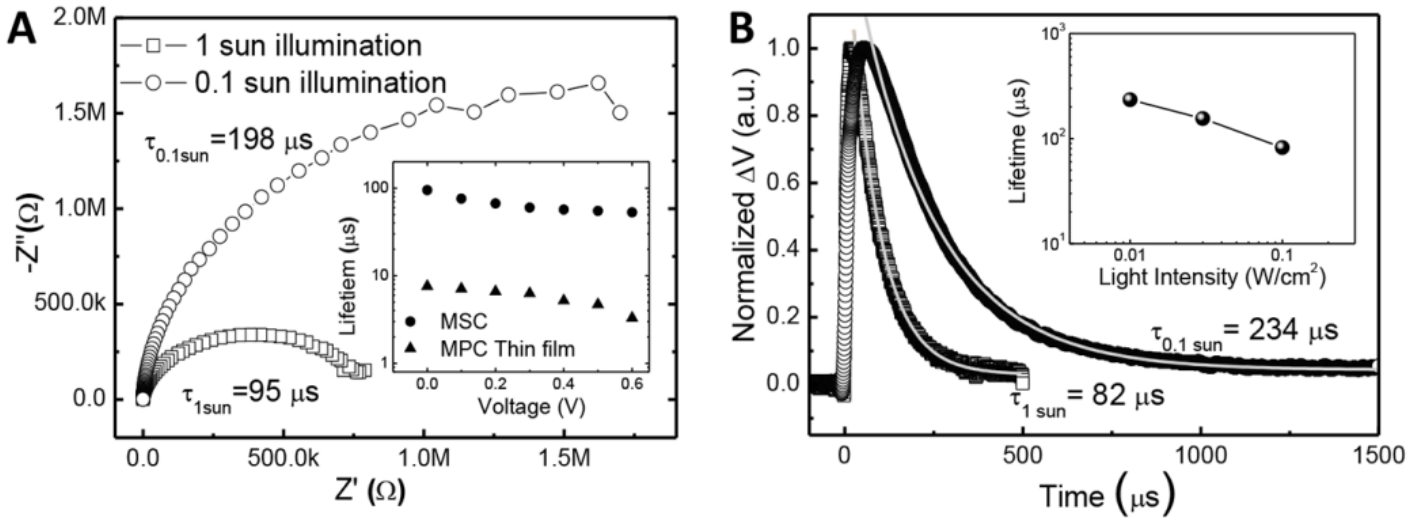

Fig. 4. Carrier recombination lifetime characterization of MSCs. (**A**) The impedance spectroscopies and (**B**) the transient photovoltaic curves of the MSC devices under one sun (square line) and 0.1 sun (circle line) illumination, respectively, with incident light from the semitransparent Au anode. The TPV decay curves were fitted by a single exponential decay function. The inset of (A) is the extracted charge recombination lifetime from IS measurement of the MSC device (solid circle) and the MPC thin film (solid triangle) at various applied voltage biases under one sun illumination. The inset of (B) is the extracted charge recombination lifetime from TPV measurement of the MSC device under various light bias intensities.